Pixel-level modelling and verification for the Euclid VIS CCD

A. Clarke*[a], D. Hall[a], N. Murray[a], J. Gow[a], A. Holland[a], D. Burt[b].
[a]centre for electronic imaging, The Open University, Walton Hall, England.
[b]e2v Technologies Plc. Chelmsford, England.

ABSTRACT

Euclid is an M-class mission selected for the next phase of ESA's long-term Cosmic Vision programme. The mission's primary aim is to provide insight into the physical cause of the accelerating universe which will be achieved by investigating the nature of dark energy, dark matter and gravity. The investigation will involve the measurement of the effects of intervening gravitational potentials on visible light from distant galaxies, a process known as weak gravitational lensing.

The CCD273 was designed by e2v for the Euclid mission, and is based on an older design for the CCD204, with changes designed and implemented to improve operation under irradiation. These changes include a narrower buried channel in the serial register to reduce trap interactions during readout. Pixel level models have been developed to improve knowledge of charge packet distribution within the CCD273 and CCD204 using Silvaco TCAD, enabling more effective predictions to be made about device functionality before and after irradiation which can be immediately tested on both devices.

This paper is focussed on latest results, with particular reference to the on-going model verification, designed to build confidence in the device models and provide feedback to further improve the modelling effort.

Keywords: Euclid, Modelling, CTI, CTE, Charge packet, CCD273, CCD204.

1. INTRODUCTION

Euclid is a space borne survey telescope which is currently being developed by the European Space Agency (ESA). The primary goal of the Euclid mission will be to aid the understanding of the expansion of the universe, through an investigation into dark matter, dark energy and gravity[1]. The mission will use a number of techniques to this end, but the VIS imager will be optimised for a weak lensing survey. Euclid's VIS imager[2] will be made up of an array of 36 4k x 4k CCD273s, which have been developed specifically for the Euclid mission by e2v technologies (UK).

Gravitational lensing is a technique developed to determine the distributions and densities of matter which lies between an observer and a distant light source[2]. The gravity of any intervening matter adjusts the path of the light from the distant source, causing a distortion in the observation (lensing). Weak gravitational lensing is an effect which causes much more subtle distortions, such as slight changes to galaxy shapes and point spread functions (PSFs)[2].

The weak lensing measurements require an unprecedented accuracy for the instruments used. Unfortunately the space radiation environment degrades the performance of the detectors over time, so characterising, modelling and understanding the effects of radiation damage in the Euclid VIS detectors is essential to mission success.

This paper is focussed on the verification of 3D TCAD models which were developed for the CCD273/CD204 and their use in understanding the degradation in charge transfer efficiency as radiation dose increases.

2. RADIATION DAMAGE

The space radiation environment can present a large concentration of high energy protons, depending on the solar cycle. Protons incident on a silicon substrate can cause displacement damage in the silicon lattice, where silicon atoms will become displaced from their lattice positions. A large portion of proton interactions will result in no damage to the detector where the displaced silicon atom finds its way back to its lattice site. However in a few instances the vacancy may migrate away from the initial lattice position until it becomes stable[9].

There are several vacancy combinations which can become stable, but one of the most problematic for n-channel CCDs is the Phosphorus-Vacancy (P-V) centre, which tend to occur within the buried channel where charge is collected and transferred. P-V centres, along with other defect types such as the di-vacancy, introduce extra energy levels into the silicon band-gap. These extra energy levels act as electron sinks, trapping and releasing electrons from passing charge packets and thus reducing the efficiency of the charge transfer process[4, 8].

The ability of radiation induced defects to trap charge is determined by Shockley-Read-Hall theory, which describes the relationship between the charge density, temperature, dwell time and the defect parameters such as capture cross section in order to calculate a capture probability[4]. By using the TCAD device models to determine charge distribution at a given signal level the portion of the buried channel which is occupied by charge, at a concentration high enough for trapping to occur, can be determined. The simulated charge distribution can be related to the CTE measurements made in the test camera as charge capture ultimately depends on a trap coming into contact with the charge packet.

3. CHARGE TRAPPING

Shockley-Read-Hall (SRH) theory describes the probability of a specific trap type capturing charge from a charge packet based on the charge density in the vicinity of a trap[4]. The trapping probability is plotted for a common trap type (the di-vacancy) in Figure 1 and differs depending on the serial or parallel transfer direction, due to the difference in the clock timings for each of these registers. The serial register dwell time tends to be of the order of 1μs, whereas the parallel register dwell time tends to be in the order of 1ms. The density at which trapping is considered probable differs depending on the dwell time, the time which the charge packet will be in contact with the trap[5].

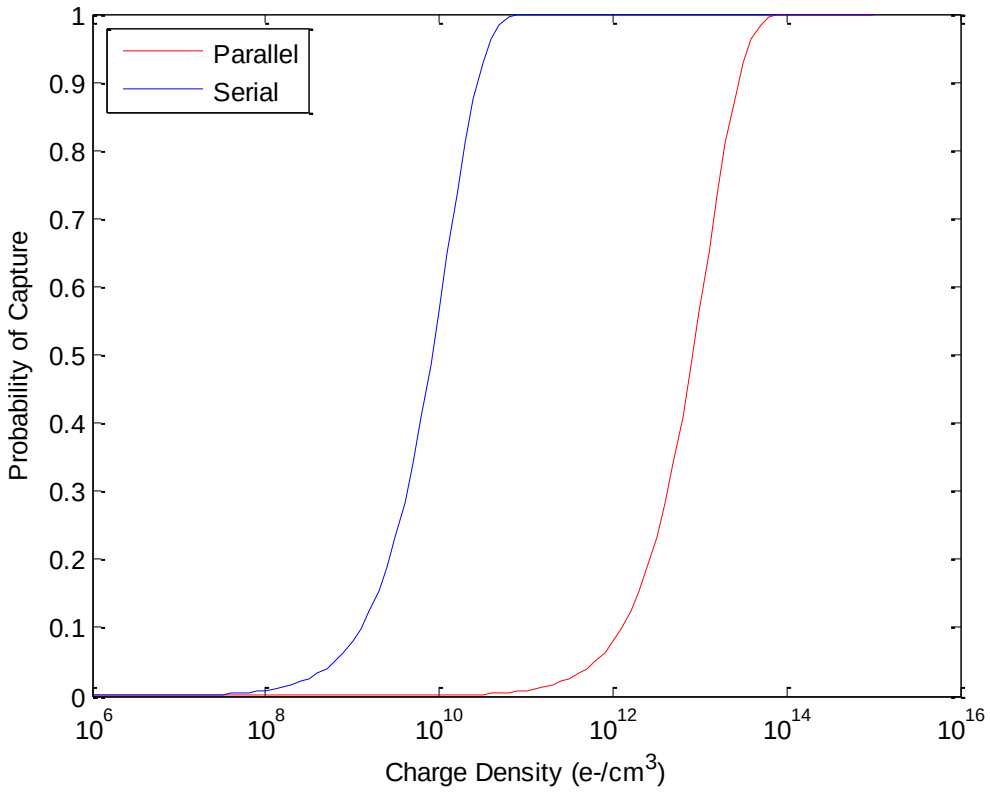

Figure 1: Trapping probability calculated for the PV centre trap (σ=5x10^{-15} cm^2) depending on the charge dwell time/trap energy. Dwell times of t=1x10^{-3}s and t=1x10^{-6}s are plotted to reflect the readout speeds of the parallel and serial registers.

The simulated charge packets are output as charge density versus position, so the trapping probability is used to determine the edges of the charge packets and hence calculate the "effective" charge packet volume. The effective volume is the volume which will have some effect on CTE through the charge–trap interaction, where within the calculated volume the probability of capture is considered high and outside the probability of capture is considered negligible.

4. CHARGE PACKET MODELS

The pixel and readout register structures from both the CCD273[3] (Euclid detector) and the CCD204 have been modelled. These devices share the same design criteria, doping specifications etc., with the only differences between the devices occurring in the electrode and doping geometry in the serial (readout) register.

The electrode configuration determines the lateral extent of the potential wells, and hence the distribution of charge during image integration and readout. These devices are modelled using Silvaco TCAD, which solves a discretised version of Poissons equation over a 3D mesh to calculate the potential field. Charge continuity equations are applied to the solutions to determine the corresponding charge density and distribution as determined by the electrostatic potential fields.

The simulated charge distributions present a "charge cloud", where the charge density reduces at the edges of the packet over a finite distance, from the higher density packet core. The simulations are then analysed using Shockley-Read-Hall (SRH) theory to determine the concentrations at which trapping is considered probable, Figure 1. These calculations make it possible to estimate the "effective" volume which a charge packet will occupy, that is, the volume within which charge concentration is high enough for trap interaction to occur and will therefore affect charge transfer efficiency. The volumes calculated for the CCD204 Pixel and Register structures follow a trend described in Clarke *et al*. 2012[7] and an example is presented in Figure 2 over a range of signal sizes.

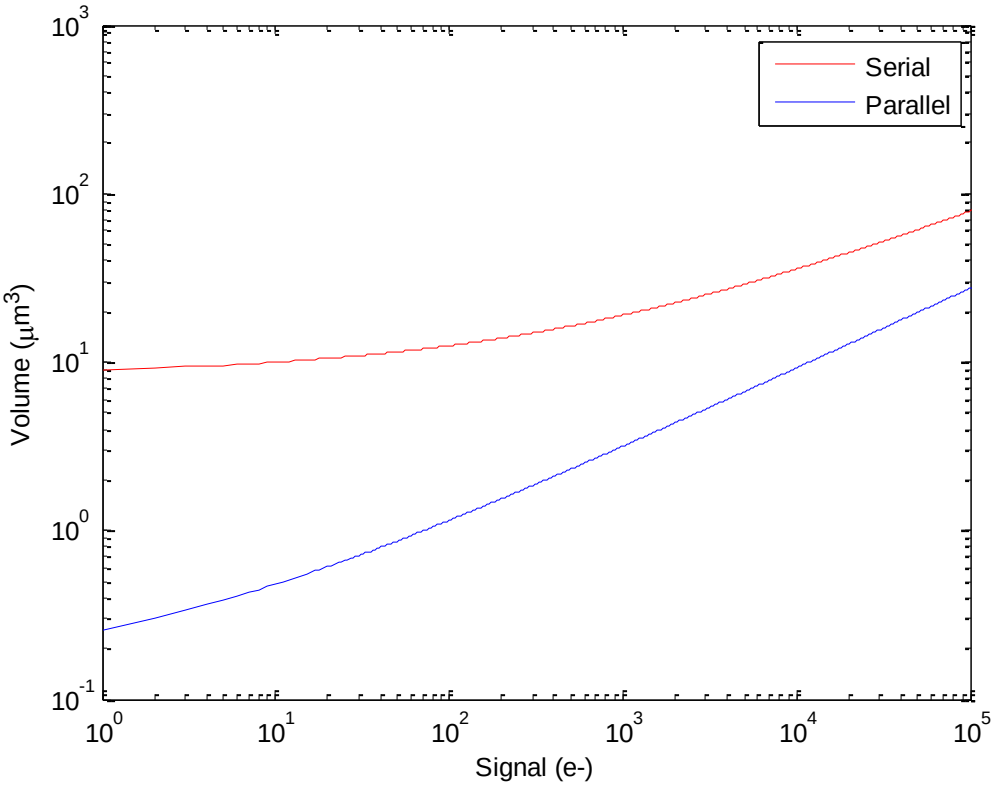

Figure 2: Comparison of the fit-lines which describe the signal-volume relationship calculated from device simulations of both the parallel and serial registers presented by Clarke 2012[7]. These take into account the difference in trapping probability between the two structures.

The volume which the charge packet occupies has a non-linear dependence on signal size. As such, charge packets tend to be disproportionately large at small signal levels in all geometries modelled (although the effect is more severe in larger structures), which indicates a much lower average charge density at small signal. As the signal level increases, both the density of the charge packet and the volume occupied by it increase. Assuming bulk traps are uniformly distributed, there will be a larger number of traps per electron at small signal levels which may cause the commonly reported increase in CTI at small signal levels [8, 9].

Taking the volume information for both the pixel and register structures, it is possible to directly compare the difference in volume across the signal range. The active area, as determined by the active electrode geometry and the buried channel width, is ~48 µm^2 in the parallel register and ~150 µm^2 in the serial register. Therefore the difference in active area should equate to a ~3x difference in charge packet volume, if a simple relationship between gate geometry and packet size is assumed. Figure 3 shows the comparison between the charge packet volume distributions calculated for the two structures, from Figure 2.

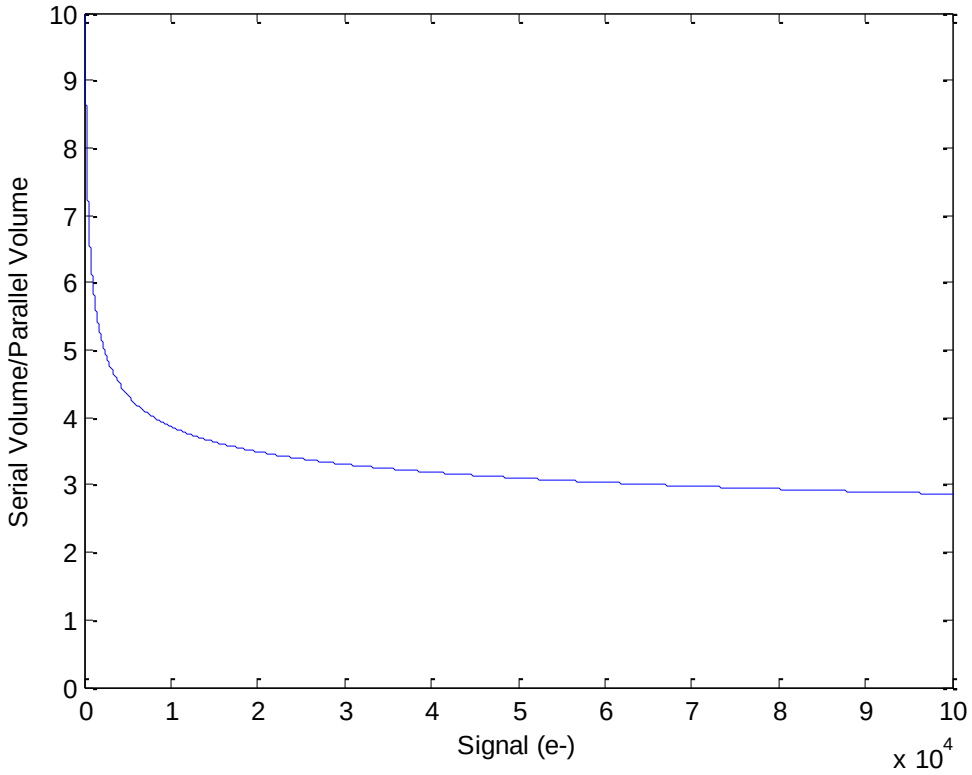

Figure 3: Difference between the volume of the charge packet calculated between the parallel and serial registers of the CCD204. These have a ~3x difference in active electrode area, but the charge packet volume actually varies depending on signal level and structure size, so only tends towards a ~3x difference at large signal levels.

Figure 3 shows that the difference in charge packet volume is very large at small signal levels. As the signal size increases the difference in volume between the structures approaches the ~3x difference which might be expected if a simple proportional relationship between electrode size and charge packet volume existed. At small signal levels charge tends to spread out along equipotential field lines, forming large, low density charge packets. In larger structures these areas of equal potential are much larger so that the small signal spreading is dependent upon the size of the structure where it is collected. As signal size increases so do both the charge density and the volume occupied by the charge packet and the difference observed between the two structures reduces.

5. TEST DEVICES

The CCD273 which will be used in the Euclid VIS detector is based on the design of the CCD204. These devices share much of the same design criteria, with the main difference in the way the readout (serial) register electrodes and channel doping are laid out. The serial register in the CCD273 is redesigned to make it narrower when compared to the CCD204. The narrowing of the readout register is introduced to improve the serial CTE. It has been suggested that the smaller channel will result in a charge packet confined to a smaller volume, and hence trap interactions will be reduced accordingly.

During the course of this work the pixel structure, which is shared between the CCD273 and the CCD204, has been modelled along with the serial register structures for each device. The models allow the simulated charge packets to be analysed and the volumes which they occupy to be determined[7]. Here we focus on further verification of the models and how charge distribution may be related to CTE measurements to test their reliability.

This paper presents Extended Pixel Edge Response[9, 12] (EPER) CTE measurements made using a CDC204 test camera, in an effort to develop more confidence in the charge packets simulated in the device models. The EPER measurements are performed over a range of signal sizes in the CCD204, with future work planned involving a repeat of these measurements on a CCD273 for comparison.

5.1 Test Camera

During these tests the CCD was mounted at one end of a small vacuum chamber where it was cooled using a cold-finger, cryo-tiger combination. The device was held at a temperature of -110°C to suppress dark current generation. An array of LEDs is located at the opposite end of the vacuum chamber which provides an option of using a range of different wavelengths for illumination. During these measurements a single LED is used, which is in the red light range at a wavelength of 660nm, the signal linearity using this LED is shown in Figure 4.

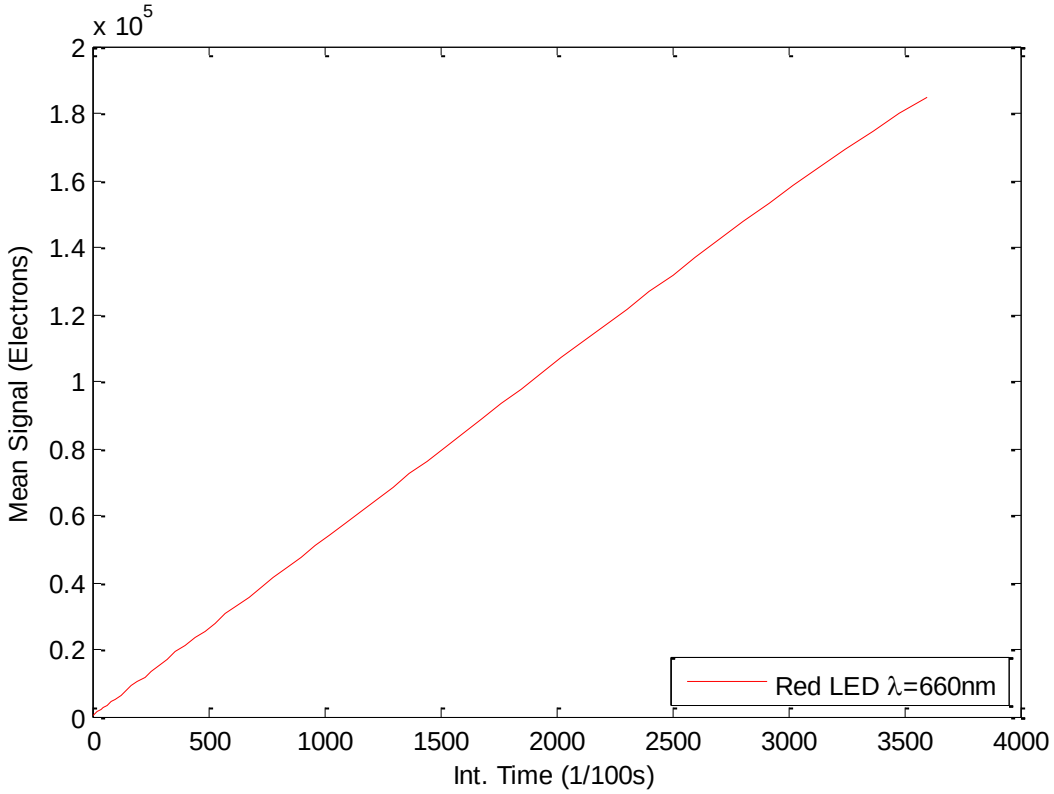

Figure 4**:** Signal level linearity produced by the red LED for a 100x100 pixel region of interest defined in the image area of the test device.

The LED illuminates the detector for the entire integration period, with larger signal levels produced by increasing the length of the integration period. The LED used to create the flat fields produces a very linear signal response over the range of the integration times tested, up to the FWC of the detector which is ~190k e-.

The LED used for illuminating the CCD provides an approximate flat field as shown in Figure 5. There is a slight illumination gradient across the detector, getting brighter in the lower right corner, which may affect the EPER measurements. The detector used for this study is a radiation damaged, engineering grade device which has been previously used for radiation damage assessments and characterization[9]. Also visible in Figure 5 are several defects present in the detector array, the most obvious in the lower right corner. There are also several bright columns and rows throughout the image area which are not visible in Figure 5.

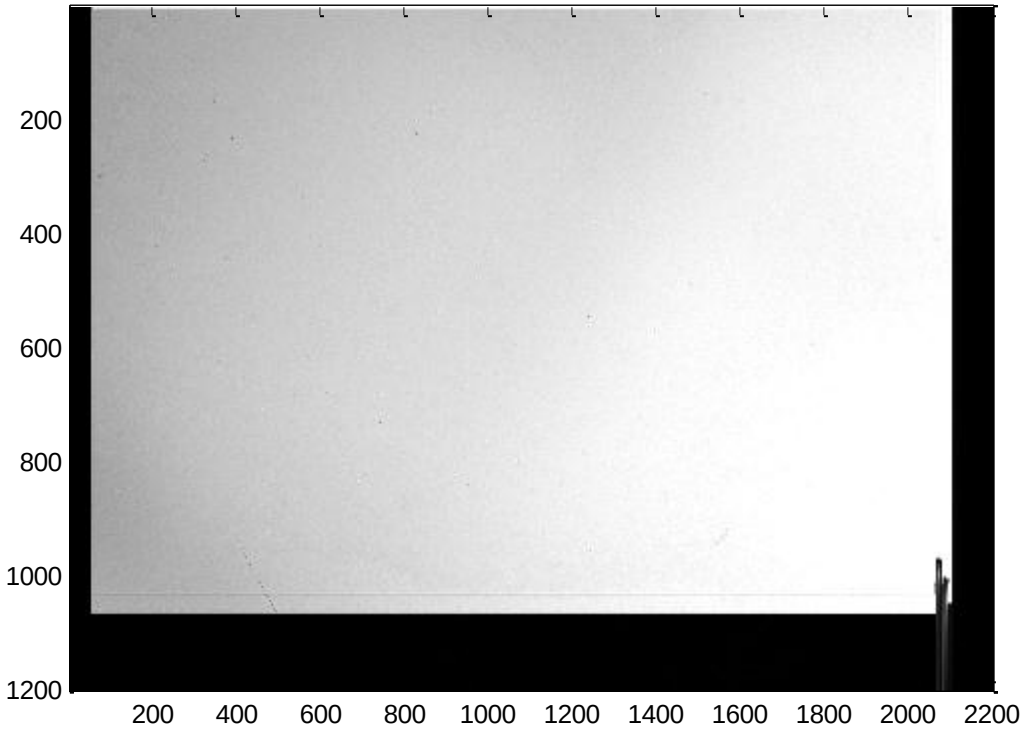

Figure 5**:** An example flat field taken using the red LED mounted in the vacuum chamber, showing the illumination gradient and areas of parallel and serial overscan. Some defects are visible in the image.

The gradient in the flat field illumination may have some detrimental effect on the accuracy of the EPER measurements, thus the CTI is measured for individual rows and columns. To reduce the noise on these measurements 100 frames, similar to the frame in Figure 5, are captured at each signal level which are averaged together before CTI is calculated using the EPER technique. The EPER calculation is repeated for each of the averaged flat fields to calculate CTI over a range of signal levels.

6. CHARGE TRANSFER INEFICIENCY

Charge transfer efficiency, CTE, is a measure of the amount of charge which is successfully transferred between pixels during the readout process. CTE is an important parameter, because even small inefficiencies can be magnified over thousands of transfers which may be required to readout a large CCD. For scientific buried channel CCDs CTE is commonly in the range of 99.999%, for convenience the inverse term CTI is generally used which is in the range of $1x10^{-5}$. It is essential that CTI is studied in detail for the Euclid detectors, because it can cause a reduction in signal level in the case of long emission-time traps, or distortion to captured images in the case of short emission-time traps. Faster emitting traps will tend to emit their captured charge into a pixel adjacent to the source, potentially causing a "charge tail" in the image[8]. Charge tails will cause distortion to galaxy shapes and PSFs which will reduce the accuracy of Euclid's weak lensing survey[11].

6.1 Extended Pixel Edge Response

Extended pixel edge response, EPER, is a technique used to indirectly calculate a value for CTI. This is achieved by measuring the amount of deferred charge in the serial and parallel overscan in a flat field image. The EPER measurement method cannot detect absolute or long time period losses from the charge packets, so it is used only as an estimate of CTE. However, EPER measurements are useful for determining general trapping information and relative CTI in CCDs.

The flat field measurements allow the illumination level to be easily varied through longer integration periods. Using flat fields in the EPER measurements allows simple CTI measurements over a large signal range.

A flat field illumination results in a similarly sized charge packet in each of the pixels of the CCD array, subject to a Poisson variance of $\sigma^2=N_e$, where N_e is the signal size. As charge packets at the same signal level should have the same volume and density characteristics, interaction with the same traps will occur repeatedly during image integration and readout. This allows the interacting traps to reach a steady state of occupancy[9], that is, if those traps emit their captured charge within the frame readout time, they will recapture charge from the current charge packet in the pixel. This will repeatedly occur until all of the flat field pixels have been read-out allowing traps to emit their captured charge into the trailing "virtual pixels".

"Virtual pixels" are the areas of serial and parallel overscan, where the clocking scheme used to transfer charge out of the device is continued after the full frame has been read out to obtain the overscan elements. The traps which have previously reached a steady state will begin to emit their captured charge into the trailing virtual pixels. This "deferred charge" alters the overscan signal level in the first overscan elements and is used to calculate CTI, through Equation 1[12]. The amount of deferred charge is related to the number of traps which have been interacting with the charge packets, and this in turn is related to both the volume and density of the charge packet and the distribution of traps. Equation 1 is used to calculate CTI from the deferred charge, where S_D is the deferred charge over the 50 overscan pixels, S_{LC} is the signal level in the last pixel of the image area and N_P is the number of pixels (or transfers) which make up the particular row or column being measured.

$$CTI=S_D/(S_{LC} \times N_P) \quad (1)$$

In these results the first 50 virtual pixel elements are summed to calculate the deferred charge, this is compared against the charge level in the last pixel of the image array and the number of pixel transfers in that dimension. One hundred images are taken and averaged at each signal level so that the CTI can be determined for each row and column individually. By averaging many frames in this fashion, the noise on the data can be reduced to obtain more accurate estimates for the level of deferred charge and the signal level in the last pixel.

6.2 Measurements

Figure 6 shows a typical column taken from the averaged image in one of the un-irradiated control regions, which is calculated from 100 flat field images, and used to calculate parallel CTI using the EPER technique. This particular column has some bright rows but the variation from pixel to pixel is very small. The signal level in Figure 6 is towards the lower end of the signal range which can be handled by this detector (FWC~190k e-) and so the deferred charge tail in the overscan region (>row number 1064) used to calculate the CTI is not visible to the naked eye.

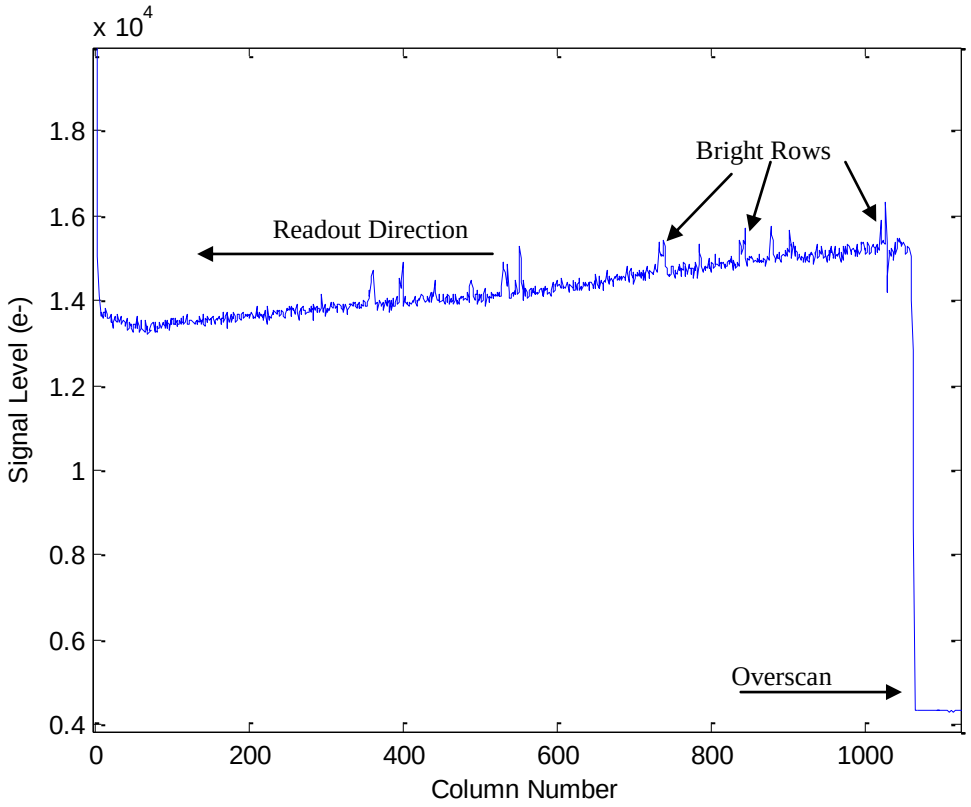

Figure 6: A typical column taken from the averaged image in an un-irradiated region of the detector. This can be used to calculate the parallel CTI of the CCD204 detector. The overscan area starts at row number 1065.

Similarly Figure 7 shows a typical row from the averaged image frame. This row shows a bigger gradient in the illumination level than the column in Figure 6 due to the non-uniform illumination provided by the LED. Also visible in Figure 7 are several bright columns, many more than are present in Figure 6. The bright columns just before the OS pixels are caused by the defect seen in the flat field illumination, Figure 5. These bright defects may reduce the reliability of the serial CTI calculations made using the EPER technique for this detector.

Another factor to note is that the test device has previously been used in a radiation test campaign during the Euclid development. As such there are areas of the device which have been irradiated with protons up to the end of life dose. This will have minimal impact on the parallel CTE measurements because these can be taken from a column in one of the un-irradiated control regions. However, the irradiated regions extend across the readout register, so are unavoidable in serial measurements.

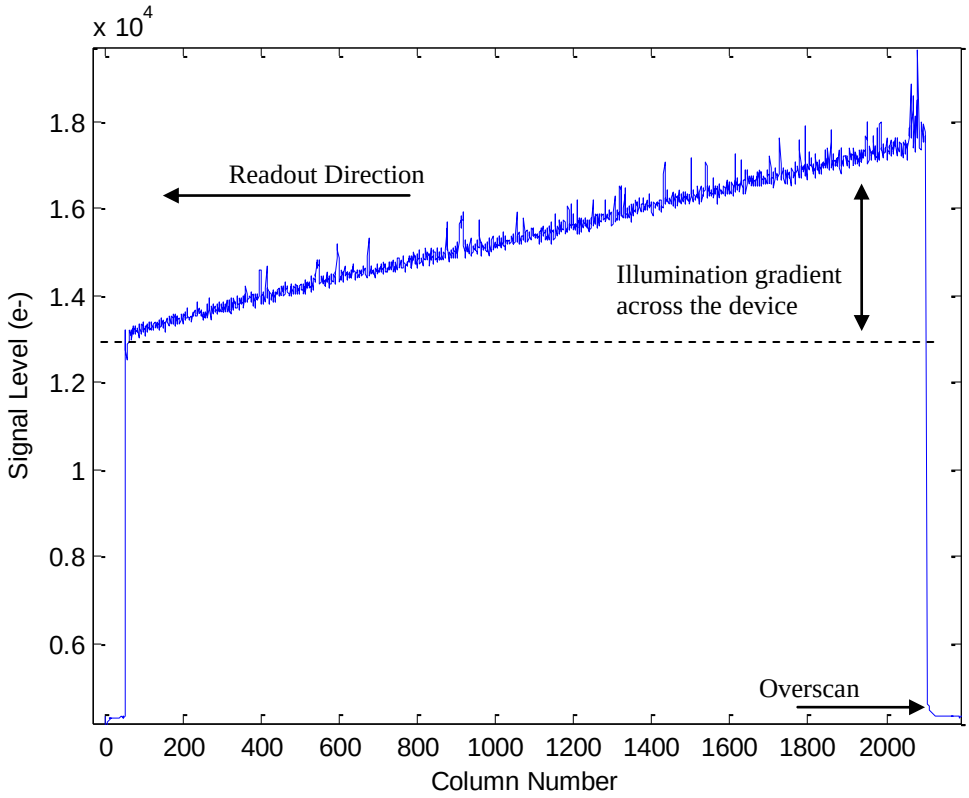

Figure 7: A typical row taken from the averaged image, which is used to calculate the parallel CTI of the CCD204 detector, showing several bright rows which occur just before the overscan section which may affect the EPER measurements. As this is from the serial register the charge will pass through several irradiated regions upon readout.

A gradient is present in the illumination level and is clearly visible in Figure 7. This will only have a small effect on the EPER measurements as the difference across the detector is small ~400 e- and the EPER calculation, Equation 1, uses the signal level of the last pixel before the overscan region.

A small EPER tail is visible in the overscan region of Figure 7, even though it comes from the same small signal flat-field frame as Figure 6. This is because the CTE is much worse in the serial dimension and limits the overall CTE of this CCD. An attempt to improve the serial CTE was one of the reasons for the redesign between the CCD273 and the CCD204. During serial transfer, the irradiated regions of the CCD are unavoidable as they overlap the serial register. The irradiated regions will increase trap interaction in the serial register.

The CTI as calculated over a range of signal sizes using the EPER technique and the results are presented in Figure 8. These are the results from a single row, for the serial CTI and a single column, for the parallel CTI. The CTI is plotted against the signal level, which is the signal value from the last pixel in the row/column before overscan.

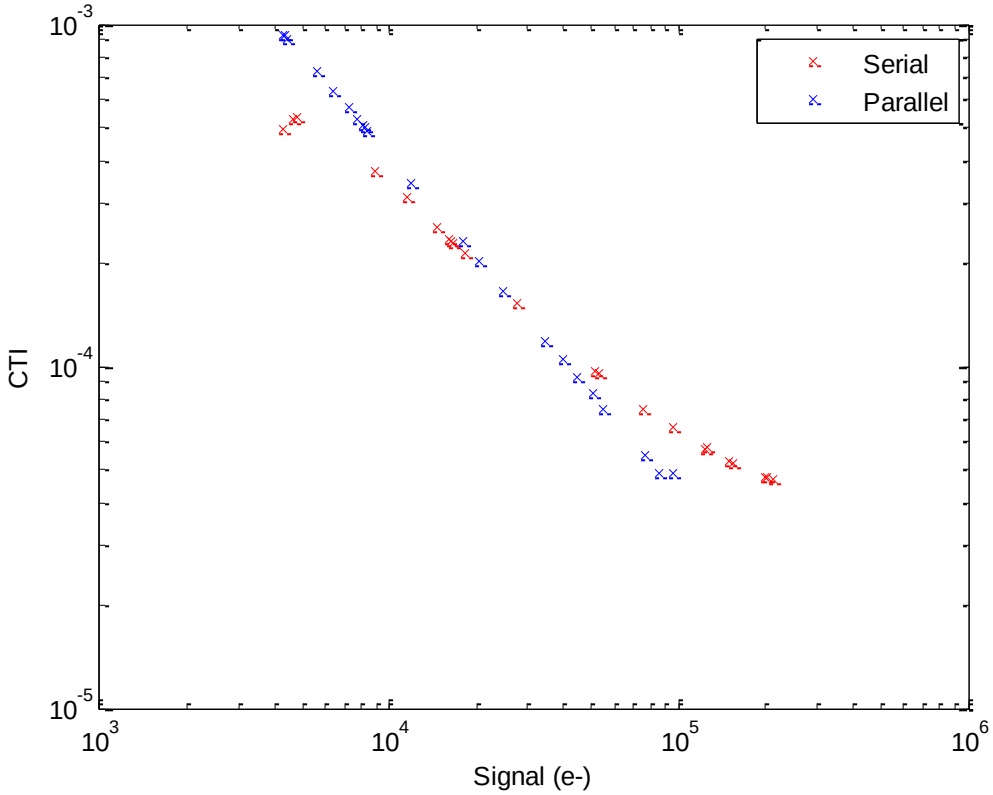

Figure 8: Charge transfer inefficiency calculated using the EPER technique from flat fields over a range of signal sizes. CTI is very high at small signal before reducing to an approximately constant value for large signals.

CTI is generally reported to be worse at small signal levels[8] and this trend is confirmed in Figure 8 where the CTI has been calculated in both the serial and parallel registers. This agrees with the volume models which suggest charge packets occupy larger volumes relative to signal size at small signal levels, which will result in more electrons per trap, assuming the traps are uniformly distributed.

Although the general trend in Figure 8 seems to agree with the other studies, however the serial CTI may be affected by the irradiated regions which the charge has to pass through during readout. Figure 8 shows CTI is better in the serial register than the parallel register at small signal, and the trends cross at a signal level of ~20k e-. Previous studies have shown proton irradiation to increase the CTI in CCDs, so the serial data, which passes through several irradiation regions during readout, may be offset from the original (un-irradiated) position in the y-axis. This prevents a reliable comparison between the serial and parallel CTI trends with this data.

7. CONCLUSIONS

Increases in charge transfer inefficiency are commonly related to charge being trapped by bulk traps, which are caused by radiation damage. Trapping theory, described by SRH, determines the probability of trapping based on charge packet density as well as the cross sections of the traps. However trapping can only occur if charge and a trap come into contact, thus the distribution of charge within the structure will also play a role.

The Silvaco simulations determine charge distribution based on the calculated electrostatic field within a 3D modelled structure to determine the position and concentration of charge packets. The signal-volume models derived from the Silvaco simulations offer the ability to predict a charge packet volume within which charge concentration is high enough for trap interaction to occur. As the transfer timings in serial and parallel registers differ, so do the charge densities which may affect trapping.

EPER measurements are calculated from the deferred charge tails in the overscan regions of flat field images, and as such offer a simple means for estimating the CTI across a range of signal levels. The volume models derived from the Silvaco device simulations show a large volume in proportion to signal size at small signal levels, resulting in a large but lower average density charge packet. The models suggest that both the average density over the charge packet, and the volume of the charge packet change with signal size[5,7].

The EPER measurements show CTI is worse at small signal which is in agreement with the literature[9]. The disproportionately large charge packets indicated by the modelling work at small signal which may contribute to the poor CTI at small signal. Transfer timings differ across the serial and parallel registers, and the dwell time of a charge packet will affect the probability of trapping. The difference in transfer timings was taken into account when the volume was calculated, so that all traps encountered by these charge packets are likely to trap.

Unfortunately a reliable serial CTI measurement was not possible because several irradiated areas are present in the serial register which will affect the CTI measurement by introducing more traps into the transfer path. The serial data trend may be shifted in the y-axis due to the radiation damage in the serial register. Further investigations are necessary to strengthen the links between charge packet models and CTE measurements.

8. REFERENCES

[1] Laureijs, R. et al. “Euclid: ESAs mission to map the geometry of the dark Universe” Proc. SPIE Vol. 8442 (2012).

[2] Cropper, M. et al. “VIS: the visible imager for Euclid” Instrumentation and Methods for Astrophysics. arXiv:1208.3369v1.

[3] Endicott, J. et al. “Charge-coupled devices for the ESA Euclid M-class mission” Proc. SPIE Vol. 8453-3 (2012).

[4] Shockley W. and Read W. T. Jr., “Statistics of the Recombinations of Holes and Electrons”, Physical Review, 87(5), 835-842 (1952).

[5] Hall, D. et al. “Modelling charge transfer in a radiation damaged charge coupled device for Euclid”. Proc. SPIE Vol. 8453 (2012).

[6] Website: “http://www.silvaco.com”. Silvaco Inc.

[7] Clarke, A. et al. “Device modelling and model verification for the Euclid CCD273 Detector” Proc. SPIE Vol. 8453 (2012).

[8] Hopkinson, G. et al. “Proton Effects in Charge-Coupled Devices” IEEE Trans. On Nuclear Science Vol. 43 No.2 (1996).

[9] Waczynski, A. et al. “A comparison of the charge transfer efficiency measurement techniques on proton damaged n-channel CCDs for the Hubble space telescope wide-field camera 3” IEEE Trans. On Nuclear Science. Vol. 48 No.6 (2001).

[10] Gow, J. et al. “Assessment of space proton radiation-induced charge transfer inefficiency in the CCD204 for the Euclid space observatory” JINST Vol. 7 (2012).

[11] Rhodes, J. et al. “The effects of charge transfer inefficiency on galaxy shape measurements” Astronomical Society of the Pacific. Vol.122 No.890 (2010).

[12] Janesick, J. “Scientific charge coupled devices” SPIE Pub. (2001).